Development of a Humanoid Dual Arm System for a Single Spherical Wheeled Balancing Mobile Robot*

Roberto Shu† and Ralph Hollis†

***Abstract*— This paper presents a new 14-DoF dual manipulation system for the CMU ballbot. The result is a new type of robot that combines smooth omnidirectional motion with the capability to interact with objects and the environment through manipulation. The system includes a pair of 7-DoF arms. Each arm weighs 12.9 kg, with a reach of 0.815 m, and a maximum payload of 10 kg at full extension. The ballbot's arms have a larger payload-to-weight ratio than commercial cobot arms with similar or greater payload. Design features include highly integrated sensor-actuator-control units in each joint, lightweight exoskeleton structure, and anthropomorphic kinematics. The integration of the arms with the CMU ballbot is demonstrated through heavy payload carrying and balancing experiments.**

I. Introduction & Related Work

The CMU ballbot, previously equipped with simple 2-DoF arms [1], shown in Fig. 1(a), has been demonstrated to be a very capable and exciting robot that has particular relevance to the field of physical human robot interaction. It is a dynamically-stable (DS) single spherical wheeled mobile robot with omnidirectional motion and intrinsic compliance. In contrast to traditional statically-stable (SS) mobile manipulators like the Willow Garage PR2 robot [2], CMU Herb robot [3], and Rollin' Justin from DLR [4], the ballbot does not have a wide and heavy base to support the arms and provide stability.

Examples of recent work on two-wheel mobile manipulators that are DS along a single axis are NASA's Robonaut [5], Golem Krang [6] and uBot-7 [7]. Like the ballbot, they require active control to keep upright, have the benefit of a small footprint, and allowance of a high center-of-mass (COM). However, they are not omnidirectional. They need to turn before moving in any direction, making it hard to navigate in tight environments.

The CMU ballbot has demonstrated reliable balancing and navigation over long distances while transporting heavy masses at speeds up to 1.5 m/s [8], [9]. It is also capable of assisting humans in sit-to-stand maneuvers where forces up to 120 N can be applied by leaning up to 15° from vertical [10]. However, the simple 2-DoF arms severely limit the range of tasks it can perform. In this paper, we present a new high performance multi-DoF pair of arms for the CMU ballbot, Fig. 2(b). The new arms increase the ballbot's manipulation workspace, payload capacity, and dexterity.

In recent years many collaborative robotic manipulation platforms (cobots) that are intended to physically interact with humans in a shared workspace have been developed. Unfortunately, none of these commercially available robotic arms meet the requirements of scale, weight, and actuation strength detailed in section II. The ABB YuMi [11], Yaskawa MOTOMAN SDA-Series [12], KAWADA NEXTAGE [13] are examples of available dual arm systems. They can perform tasks such as loading, packing and material handling. However, they either have low payload capacity (e.g.,YuMi and NEXTAGE payload capacity ranges between 0.5 kg - 3.0 kg), or are mounted to large heavy fixed bases that make them impossible to be interfaced with the CMU ballbot (e.g., MOTOMAN dual arm system weighs 220 kg).

The KUKA LBR iiwa based on the DLR LWR III [14] and the UR10 by Universal Robots [15] are both examples of robotic arms that have high positioning precision, rich proprioception that enables the robot arms to compliantly interact with the physical world, and high payload capacity of 14 kg and 10 kg respectively. However, their usability for the enhanced ballbot is limited due to their heavy weights (LBR iiwa 29.9 kg and UR10 28.9 kg) and the need for a large separate control box that does not fit on-board. Further, the

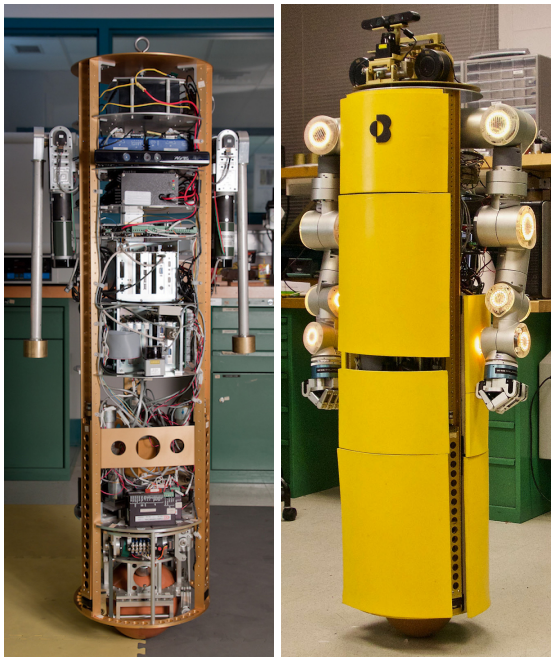

(a) (b)

Fig. 1: The CMU ballbot in its dynamically stable state with its (a) previous simple 2-DoF arms and (b) new pair of 7-DoF arms and Barrett hands in their zero configuration state.

*This work was supported in part by NSF grant CNS-1629757

† The Robotics Institute, Carnegie Mellon University, Pittsburgh, PA 15213, USA {rshu,rhollis}@cs.cmu.edu

UR10 only has 6-DoF and a non-anthropomorphic kinematic configuration. The 7-DoF Franka Emika Panda arm [16] and Kinova Gen3 Ultra lightweight [17] robotic arms are lighter alternatives. They weigh 17.8 kg and 8.2 kg, but have a limited payload capacity of 3 kg and 4 kg, respectively. The Panda arm also requires a large 7 kg external control box.

Few robotic arms have been developed in research facilities that achieve a low weight and high payload capacity, such as the KIT dual arm system [18] and the bi-manual manipulation platform by Istituto Italiano di Tecnologia (IIT) [19]. The KIT arm consists of two 8-DoF, strong (11 kg payload), anthropomorphic kinematics robot arms. The IIT system is a pair of high impact resistant 7-DoF robot arms with superior weight to payload ratio (0.85 for continuous lifting operation). The IIT arm weighs only 8.5 kg and has a maximum payload capacity of 7 kg continuous and 15 kg peak. However, both manipulation systems are assembled from non-commercial custom sensor-control-actuator units, contrary to our developed arms. Further, the KIT dual arm is heavy and large (25 kg weight per arm and 1224 mm arm reach).

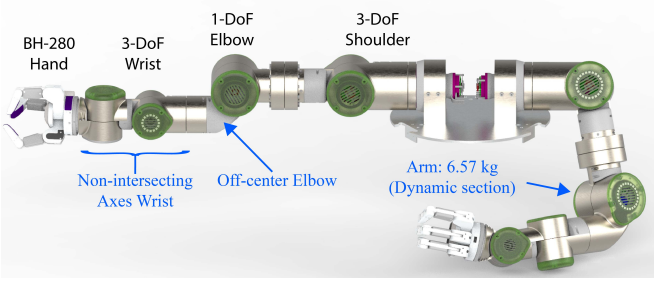

Fig. 2: CMU ballbot dual arm system with BH-282 grippers (CAD rendering).

II. System Requirements

The objective is to enhance the CMU ballbot by adding a pair of new lightweight human-scale arms/hands. Human-robot collaborative tasks benefit from rich proprioception, large payload capacity, and physical resilience—leading to the following specifications:

- High power density (weight-to-payload ratio ~1.0).
- Large payload capacity (~10 kg payload per arm).
- Lightweight to be on the ballbot (~10 kg per arm).
- Arm dimensions similar to those of the average human.
- Large bi-manual workspace similar to that of a human.
- Passive and/or active compliance, to react compliantly to unanticipated disturbances.
- Physical robustness against perturbations and impacts.
- High-resolution position, inertial and torque sensing.

The mechanical design decisions to achieve the specified requirements are detailed in the following sections.

III. Arm Mechanical Design

The developed pair of 7-DoF robot arms with human-like kinematic configuration is shown in Fig. 2. Each arm has a maximum reachable distance of 815.5 mm without an end-effector (EE) and weighs 12.9 kg with a 10 kg payload

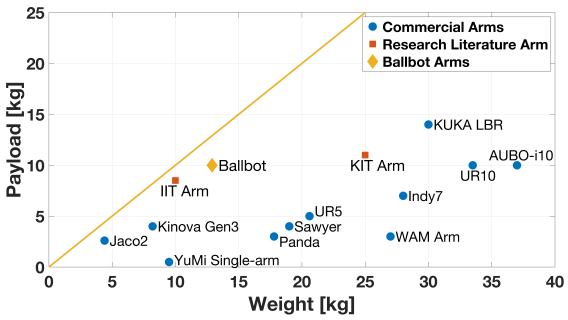

Fig. 3: Plot of arm weight vs. payload capacity for different robotic arms. Commercial and research literature arms are shown.

capacity (0.78 payload-to-mass ratio). 49.1% (6.34 kg) of the total arm mass is considered static, only 6.56 kg are dynamic, reducing the required joint torques. When compared to thirteen of the most common cobots, the ballbot arms exhibit notable weight and strength as shown in Fig. 3. Only 31% of the arms have an equal or larger payload capacity than the ballbot's arms. The KIT Arm and KUKA LBR can carry 1 kg and 5 kg more than the ballbot's arms, respectively. However, their larger payload capacity comes with significantly greater weight. These arms weigh >93% more than the ballbot's arms. The UR10 and AUBO-i10 that have the same payload capacity as the ballbot's arms weigh >159% more.

For manipulation, a Barrett Hand BH-280 [20] is attached to each arm. However, there is bolt pattern with CAN bus and 24 V interface to allow mounting of different grippers, hands, and tools to fit the task's needs. Compliant arm behavior is achieved through a lightweight structure combined with high-resolution torque sensing [21]. Recall, the ballbot itself reacts with intrinsic compliance due to its balancing controller, which will add to any compliance of the arms. To ensure physical robustness to extreme impacts, a ball-detent torque limiter in the shoulder joint decouples the joint actuator from the affected links. The arms' major components and joints configuration are summarized in Fig. 4.

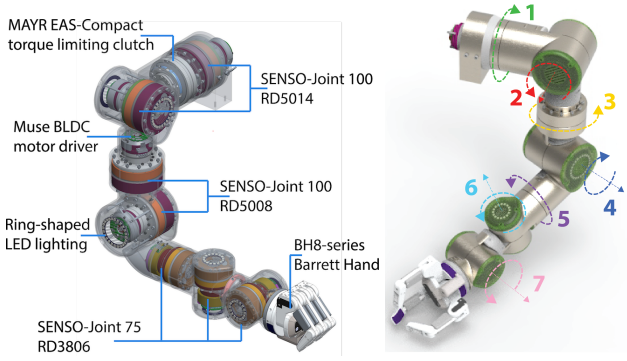

(a) (b)

Fig. 4: Overview of the CMU ballbot's 7 DoF humanoid arm: (a) major components and (b) joint configuration.

TABLE I: Human arm vs. 7-DoF robot arms dimensions.

Distance	Arms				
	Human [22] [mm]	**KIT [18] [mm]**	**IIT [19] [mm]**	**KUKA iiwa [23] [mm]**	**Ballbot [mm]**
Shoulder - Elbow	303	409	293	400	262
Elbow - Wrist	270	364	410	526	353.5
Wrist - EE Tip	137	227	–	–	120
Shoulder - EE Tip	710	1000	(703)	(926)	735.5

A. Arm Kinematics

The selected arm kinematics configuration with 3-DoF shoulder, 1-DoF elbow, and 3-DoF wrist, approximately duplicate the anthropomorphic kinematics of the human arm. With 7 DoFs, each arm can manipulate all 6 DoFs of the environment with adequate dexterity while using the additional DoF to resolve constraints introduced by the surrounding environment. To increase the elbow flexion range an off-center elbow was implemented. Similarly, a non-intersecting-axes wrist design was chosen to increase the wrist joint's range of motion. In contrast to other 7-DoF arms, the ballbot's arms are of similar scale to that of an average adult human, Table I. From shoulder to EE tip the arm measures 735.5 mm, only 20 mm more than a human arm (710 mm [22]). However, note that at full extension, from the arm base to the EE tip, the arm has a reach of 935.5 mm, but a 200 mm shoulder section is located inside the ballbot's body and reduces the effective reach to 735.5 mm. The arm dimensions are summarized in Fig. 5.

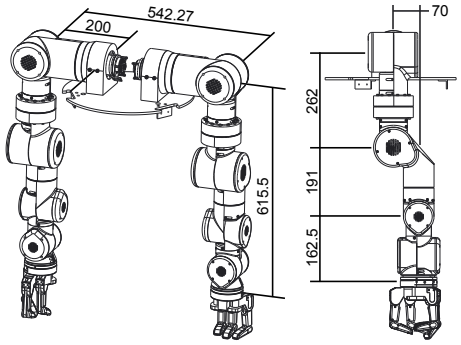

Fig. 5: Size specification for pair of arms, all dimensions in mm.

B. Range of motion and workspace

The target joint range and workspace was defined considering human ergonomic data [22]. The human arm range of motion was used as a starting point, but when possible a greater range was implemented to enhance the motion and manipulation capability of the arm. The range of the upper and lower shoulder rotations (Joint 1 and Joint 2) was extended to be capable of full 360° rotation. This, allows the ballbot to effortlessly switch between a front and back bimanual workspace in tight locomotion spaces without rotating the body. Similarly, the range of the elbow (Joint 4) was increased by implementing an off-center elbow joint arrangement that results in a 30° extension and 110° flexion. The wrist joints are arranged in a non-anthropomorphic configuration with non-intersecting axes to maximize the range of motion of the wrist flexion/extension and abduction/adduction (Joint 6 and Joint 7) motions to $[-90°, 90°]$. The range of motion for each joint is summarized in Table II. The increased range of motions allows for a greater bimanual workspace of 0.46 m^2 (Fig. 6), compared to 0.3 m^2 of the average human [22].

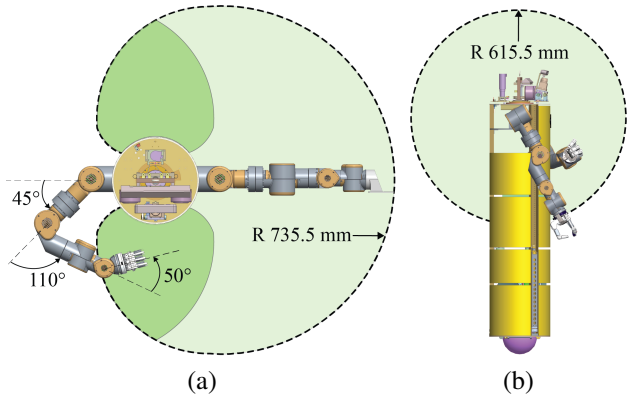

Fig. 6: Workspace of the ballbot arms: (a) top view (b) side view. Dark green represent bi-manual workspace area.

C. Actuator and motor driver selection

To determine the actuation requirements, a dynamic model of the 7-DoF arm was developed using MATLAB's Robotics Toolbox [24]. Inertia and mass properties were estimated from the CAD model. The recursive Newton-Euler algorithm was used to solve the inverse dynamics problems. A set of 30 different joint trajectories that covered the entire workspace were simulated with a 10 kg payload mass attached to the end of the arm and subject to gravity. As expected, the shoulder joints demand the highest torque (105 Nm peak). From the box plot in Fig. 7, it is apparent that joint torque requirements can be satisfied by using only three different actuators sizes with peak torques of 105 Nm, 60 Nm, and 25 Nm.

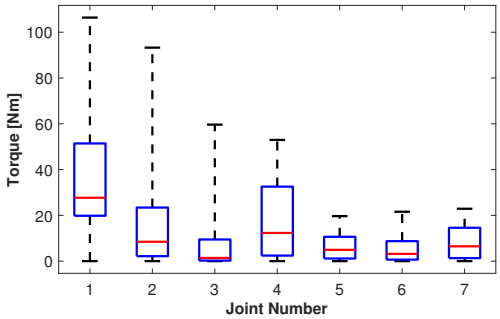

Fig. 7: Box plot of joint torques recorded from the simulated trajectories moving a 10 kg payload. The black "whiskers" show the maximum and minimum torques, the average recorded torque is shown by the red line, and interquartile range by the blue box.

The arm is built around three different sizes of sensor-actuator units by SENSODRIVE GmbH[1] (Fig. 8). The units used, *SENSO-Joint*: *100 RD5014 AEST*, *100 RD5008 AEST*, and *75 RD3806 AEST*, achieve peak torques of 120 Nm,

[1]SENSODRIVE GmbH: https://www.sensodrive.de.

100.8 Nm, and 19 Nm, respectively. Their complete specifications are summarized in Table II. Each drive unit combines a TQ-RoboDrive BLDC motor, Harmonic Drive, cross-roller ring bearing that decouples the input and output, incremental and absolute encoders, motor temperature sensor and output torque sensor in a compact lightweight package. A custom 50 mm diameter circular shape motor controller board was integrated to the back of each SENSO-Joint, eliminating the need for a large external control box. The motor controller board includes the driver electronics, 6-axis IMU sensor, as well as the communication and sensor interfaces. The only connections out of each sensor-actuator-control unit are to the DC-bus for power supply and to the Ethernet bus for communication. Those connections are daisy-chained between units and the cables are routed through the actuator's hollow shaft. This allows for $\pm 720^{\circ}$ joint rotation, minimum cables and overall smaller arm volume.

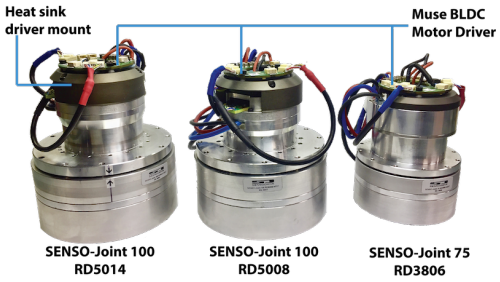

Fig. 8: SENSO-Joint sensor-actuator units from SENSODRIVE assembled with custom BLDC motor controllers by MUSE Robotics used in the ballbot's 7-DoF arm.

D. Arm Structure

The arm structure that links all the SENSO-Joint units is based on an exoskeleton approach using lightweight shell structures that are both load-bearing and covers [18], [19]. The actuators are floating inside the exoskeleton structure and are mechanically fixed to the link structure via screw flanges, as illustrated in Fig. 9.

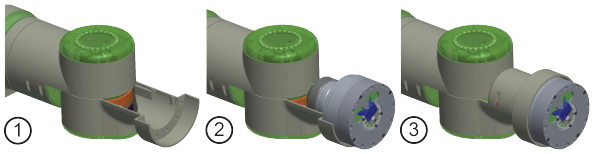

Fig. 9: Integration steps of a sensor-actuator-control-unit into the exoskeleton shell structure

The exoskeleton structure has several advantages over the classic frame construction. The bending stiffness K of a link is proportional to the material's Young's modulus E times the area moment of inertia I and inversely proportional to its length L: $K = 3EI/L^3$. Thus, the arm links can be optimized to be short hollow structures with large I with minimum openings that are lightweight while stiff and therefore increase precision.

The arm is assembled with only a few complex parts, in contrast to using many simple parts in traditional frame constructions. Loading torques and forces are only transmitted through the link's mounting flanges allowing thin wall structures with thicker flanges where loads are larger. The thin (3 mm thick walls) hollow exoskeleton links (Fig. 10) were machined from single blocks of 7075-T6 aluminum. The links weigh between 0.242 kg - 0.454 kg.

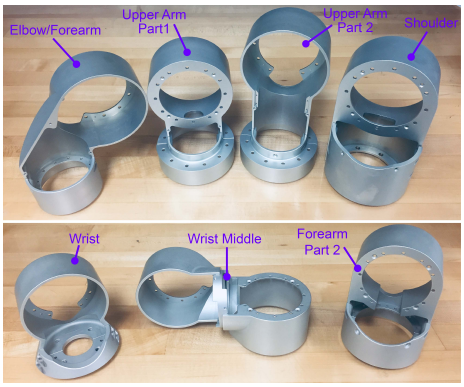

Fig. 10: Exoskeleton shell structural links. Each link is machined from a single block of 7075 aluminum using 5-axis milling.

IV. Experimental Validation

A. Arm control and actuation performance

The implemented torque-impedance based feedback controller on each arm includes feedforward gravity and torque sensing compensation, as shown in Eq. 1.

$$\boldsymbol{\tau}_d = K_{P_\alpha}(\boldsymbol{\alpha}_d - \boldsymbol{\alpha}) + K_{D_\alpha}(\dot{\boldsymbol{\alpha}}_d - \dot{\boldsymbol{\alpha}}) + g(\boldsymbol{\alpha}, \dot{\boldsymbol{\alpha}}) - \boldsymbol{\tau}, \quad (1)$$

where $\boldsymbol{\tau_d} \in \mathbb{R}^7$ is the vector of joint torque input commands, $\boldsymbol{\alpha}, \dot{\boldsymbol{\alpha}} \in \mathbb{R}^7$ are the arm joint positions and velocities, $\boldsymbol{\alpha}_d, \dot{\boldsymbol{\alpha}}_d \in \mathbb{R}^7$ are the desired joint positions and velocities, $K_{P_\alpha}, K_{D_\alpha}$ are positive definite diagonal gain matrices, $g(\boldsymbol{\alpha}, \dot{\boldsymbol{\alpha}})$ is the gravity compensation term based on the dynamic model of the arm, and $\boldsymbol{\tau} \in \mathbb{R}^7$ is the vector of measured joint torques. An overview of the complete control loop is illustrated in Fig. 11.

The joint control was implemented on an Intel Core2 Duo @ 2.4GHz, running Ubuntu 14.04 Linux. The computer calculates motor current commands and sends them to each motor driver board via an Ethernet bus running at 500 Hz with a 100 Mbps data rate. The inner PI current control loop is executed on each motor driver at 10 kHz. To ensure that no mechanical joint limits are violated during operation a unidirectional stiffening PD controller is implemented in the "Safety Check" block in Fig. 11.

Payload Manipulation: The arm's capabilities were evaluated by holding a 6.8 kg dumbbell with the 1.2 kg BH-280 hand while tracking a desired motion. Fig. 12 and the video attachment[2] show a motion from the zero configuration to elbow flexion, followed by moving the mass above the ballbot's turret, and ending with shoulder rotation at full extension. The corresponding joint torque commands are shown in Fig. 13. The required torques are significantly lower than the actuator unit limits listed in Table II. Although the arm is capable of lifting 10 kg without an EE the test was limited to 6.8 kg because it is the maximum payload the BH-280 can hold before its fingers buckle.

[2]https://youtu.be/FYKJiXFJrlE

TABLE II: Mechanical Properties of the 7-DoF Arm

Joint No.	Articulation	Range [deg.]	Actuator Type [SENSO-Joint]	Gear Ratio	Torque [N/m] peak - nominal	Max. Velocity [rpm]	Mass [kg]
1	Shoulder flexion/extension	[-720, 720]	100 RD5014 AEST	160	120 - 56	21	1.45
2	Shoulder abduction/adduction	[-10,190]	100 RD5014 AEST	160	120 - 56	21	1.45
3	Shoulder rotation int./ext.	[-720, 720]	100 RD5008 AEST	160	100.8 - 30	34	1.35
4	Elbow flexion/extension	[-30,110]	100 RD5008 AEST	160	100.8 - 30	34	1.35
5	Wrist rotation	[-720,720]	75 RD3806 AEST	100	19 - 5.4	85	0.7
6	Wrist flexion/extension	[-90,90]	75 RD3806 AEST	100	19 - 5.4	85	0.7
7	Wrist abduction/adduction	[-90,90]	75 RD3806 AEST	100	19 - 5.4	85	0.7

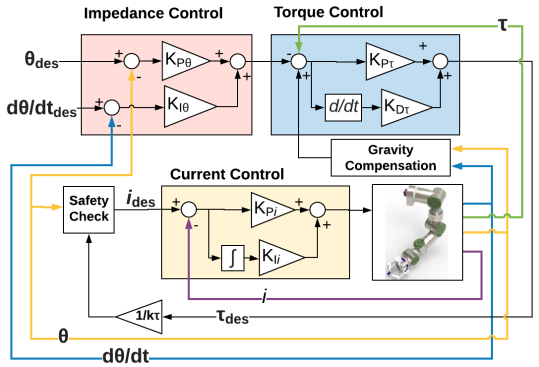

Fig. 11: Block diagram of the impedance joint controller with gravity compensation. The motor current i is measured by the MUSE motor driver board, the joint torque τ is measured by a torque sensor and the motor position θ by an absolute encoder. The derivatives are obtained by numerical differentiation.

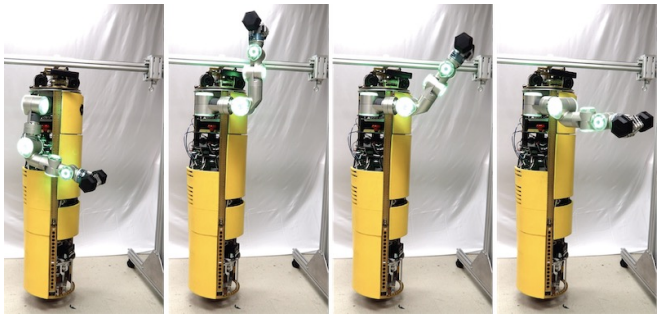

Fig. 12: Screenshots of the CMU ballbot lifting 6.8 kg dumbbell with the new arm and Barrett Hand. Here, the ballbot is constrained at the top by a fixture and is not balancing.

B. Balancing performance

The effect of the new arms on the ballbot's balancing performance was evaluated by tracking a fixed ground position while moving the arms. To perform this task a cascading PD-PID with feedforward COM regulation controller as described in [9] was implemented. In this work we use the 3D instead of 2D kinematics of the system to determine the COM position. An overview of the controller is shown in Fig. 14. The inner PID controller loop maintains the ballbot's balance by tracking desired lean angles ϕ_d. In the case of pure balancing it tracks a zero lean angle ($\phi_d = 0$). For other tasks such as lifting or navigation, a non-zero lean angle ($\phi_d(t)$) is required. The outer PD control loop computes desired lean angles to track the desired ground trajectory ($\theta_d(t)$ and $\dot{\theta}_d(t)$). The feedforward lean angle term compensates

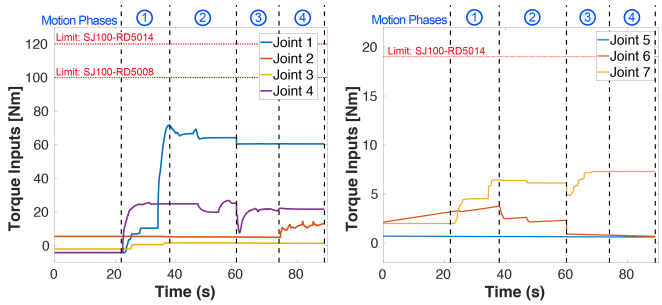

Fig. 13: Joint torque command evolution to lift a 6.7 kg payload at the end of the arm. The arm is moved from pointing straight down to fully extended, then performs a shoulder rotation at full extension.

for the robot's COM shift due to the arms' movement. The compensation lean angle trajectory is calculated through a forward kinematics analysis of the desired joint trajectory to determine the resulting COM angle offset with respect to the gravity vector. The balancing controller runs real-time at 500 Hz on a second Intel Core2 Duo @ 2.4GHz onboard computer running QNX RTOS. Successful balancing with the arms in different configurations was attained as shown in Fig. 15.

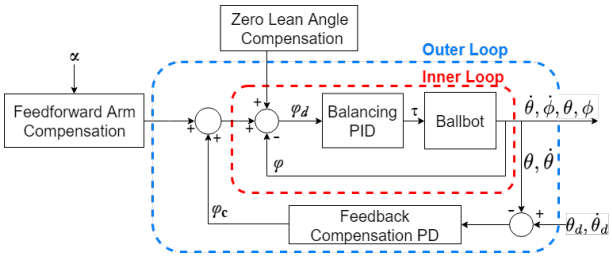

Fig. 14: Overview of the balancing cascading control loops with feedforward lean angle compensation term.

1) Single arm motion: One arm was kept stationary at the zero configuration while the other arm was commanded to full extension as shown in Fig. 15 (a). The ballbot is able to maintain its balance throughout the entire motion. With the COM regulator the ground position tracking error decreased by $\sim 87\%$ in the axis of motion, as shown in Fig. 16. Also, the oscillation of the ball position is reduced and steady state is reached faster in both axes.

2) Double arm motion: Both arms move simultaneously from pointing straight down to a 90° elbow flexion as shown

(a) (b) (c)

Fig. 15: The enhanced CMU ballbot balancing with the arms in different configurations.Here, a slack rope is attached for safety.

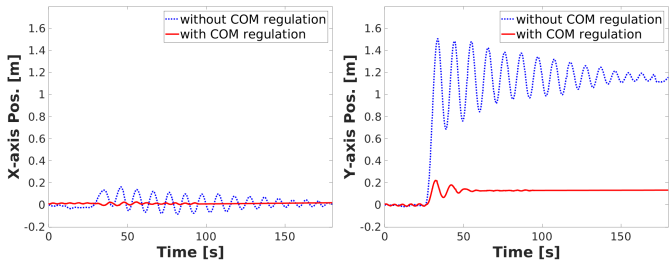

Fig. 16: The ballbot's X and Y axis position on the ground during the motion of a single arm from straight down to full extension.

in Fig. 15 (b). The ballbot is able to maintain its balance through the entire motion. Again with the COM regulator significantly decreases the ground position tracking error ($\sim 85\%$), oscillations and settling time in both axes, as seen in Fig. 17. Similarly, for the single arm motion the ball position steady-state error is <0.15 m. This error could be decreased by increasing the I term in the balancing PID and by considering dynamic effects of the arm motion.

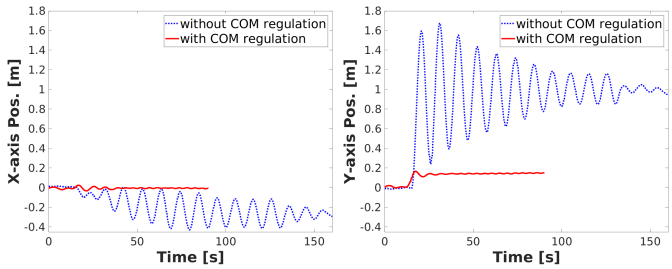

Fig. 17: The ballbot's X and Y axis position on the ground during the motion of both arms from straight down to 90° elbow flexion.

V. Conclusion and Future Work

In this paper, we introduced a new type of agile and dexterous mobile manipulator by adding a pair of 7-DoF arms and hands to enhance the CMU ballbot research platform. The developed 7-DoF arms are of comparable size and weight to that of an average adult human. We demonstrated successful control of the arms while maintaining balance. Our future research includes developing more intelligent controls that combine manipulation and locomotion to realize assistive tasks such as maneuvering a manual wheelchair, leading elderly or sight impaired individuals from place to place inside a building, and cooperative carrying of heavy objects.

References

[1] U. Nagarajan, G. Kantor, and R. Hollis, "The ballbot: An omnidirectional balancing mobile robot," *The International Journal of Robotics Research*, vol. 33, no. 6, pp. 917–930, 2014.

[2] Willow Garage. [Online]. Available: http://www.willowgarage.com/pages/pr2/overview

[3] S. S. Srinivasa, D. Berenson, Cakmak, *et al.*, "Herb 2.0: Lessons learned from developing a mobile manipulator for the home," *Proceedings of the IEEE*, vol. 100, no. 8, pp. 2410–2428, 2012.

[4] C. Borst, T. Wimbock, F. Schmidt, M. Fuchs, *et al.*, "Rollin' Justin mobile platform with variable base," in *Robotics and Automation, (ICRA) International Conference on*. IEEE, 2009, pp. 1597–1598.

[5] R. O. Ambrose, R. T. Savely, S. M. Goza, *et al.*, "Mobile manipulation using NASA's Robonaut," in *Robotics and Automation, (ICRA) International Conference on*. IEEE, 2004, pp. 2104–2109.

[6] M. Stilman, J. Olson, and W. Gloss, "Golem Krang: Dynamically stable humanoid robot for mobile manipulation," in *Robotics and Automation, (ICRA) International Conference on*. IEEE, 2010, pp. 3304–3309.

[7] D. Ruiken, J. P. Cummings, U. R. Savaria, F. C. Sup, and R. A. Grupen, "uBot-7: A dynamically balancing mobile manipulator with series elastic actuators," in *Humanoid Robotics (Humanoids), International Conference on*. IEEE, 2017, pp. 676–682.

[8] U. Nagarajan, B. Kim, and R. Hollis, "Planning in high-dimensional shape space for a single-wheeled balancing mobile robot with arms," in *Robotics and Automation, (ICRA) International Conference on*. IEEE, 2012, pp. 130–135.

[9] F. Sonnleitner, R. Shu, and R. L. Hollis, "The mechanics and control of leaning to lift heavy objects with a dynamically stable mobile robot," in *Robotics and Automation, (ICRA) International Conference on*. IEEE, 2019, pp. 9264–9270.

[10] M. Shomin, J. Forlizzi, and R. Hollis, "Sit-to-stand assistance with a balancing mobile robot," in *Robotics and Automation, (ICRA) International Conference on*. IEEE, 2015, pp. 3795–3800.

[11] "ABB's Collaborative Robot -YuMi - Industrial Robots From ABB Robotics." [Online]. Available: https://new.abb.com/products/robotics/industrial-robots/irb-14000-yumi

[12] "Yaskawa MOTOMAN SDA10D." [Online]. Available: https://www.motoman.com/en-us/products/robots/industrial/assembly-handling/sda-series/sda10d

[13] "KAWADA NEXTAGE: a next-generation robot able to work together with people." [Online]. Available: http://nextage.kawada.jp/en/

[14] G. Hirzinger, N. Sporer, A. Albu-Schaffer, *et al.*, "DLR's torque-controlled light weight robot III-are we reaching the technological limits now?" in *Robotics and Automation, (ICRA) International Conference on*. IEEE, 2002, pp. 1710–1716.

[15] Universal Robots. [Online]. Available: http://www.universal-robots.com

[16] F. E. GmbH, "Franka Emika Panda." [Online]. Available: https://www.franka.de/technology

[17] Kinova Robotics. [Online]. Available: https://www.kinovarobotics.com/en

[18] S. Rader, L. Kaul, H. Fischbach, N. Vahrenkamp, and T. Asfour, "Design of a high-performance humanoid dual arm system with inner shoulder joints," in *Humanoid Robots (Humanoids), International Conference on*. IEEE, 2016, pp. 523–529.

[19] L. Baccelliere, N. Kashiri, L. Muratore, *et al.*, "Development of a human size and strength compliant bi-manual platform for realistic heavy manipulation tasks," in *Intelligent Robots and Systems, (IROS) International Conference on*. IEEE, 2017, pp. 5594–5601.

[20] Barrett Technology. [Online]. Available: https://www.barrett.com/about-barrethand/

[21] A. De Luca, A. Albu-Schaffer, S. Haddadin, and G. Hirzinger, "Collision detection and safe reaction with the DLR-III lightweight manipulator arm," in *Intelligent Robots and Systems, (IROS) International Conference on*. IEEE, 2006, pp. 1623–1630.

[22] NASA, "Man-Systems Integration Standards (MSIS) - NASA-STD-3000." [Online]. Available: https://msis.jsc.nasa.gov/sections/section03.htm

[23] KUKA, "KUKA LBR iiwa." [Online]. Available: https://www.kuka.com/en-de/products/robot-systems/industrial-robots/lbr-iiwa

[24] P. Corke, *Robotics, Vision and Control: Fundamental Algorithms In MATLAB® Second, Completely Revised*. Springer, 2017, vol. 118.